

Ground state phase diagram of the triangular lattice Hubbard model by density-matrix renormalization group method

Tomonori Shirakawa¹, Takami Tohyama², Jure Kokalj^{3,4}, Shigetoshi Sota⁵, and Seiji Yunoki^{1,5,6}

¹Computational Quantum Matter Research Team,

RIKEN Center for Emergent Matter Science (CEMS), Wako, Saitama 351-0198, Japan

²Department of Applied Physics, Tokyo University of Science, Tokyo 125-8585, Japan

³Jožef Stefan Institute, Jamova c. 39, 1000 Ljubljana, Slovenia

⁴Faculty of Civil and Geodetic Engineering, University of Ljubljana, SI-1000 Ljubljana, Slovenia

⁵Computational Materials Science Research Team,

RIKEN Advanced Institute for Computational Science (AICS), Kobe, Hyogo 650-0047, Japan

⁶Computational Condensed Matter Physics Laboratory, RIKEN, Wako, Saitama 351-0198, Japan

(Dated: June 23, 2016)

Two-dimensional density-matrix renormalization group method is employed to examine the ground state phase diagram of the Hubbard model on the triangular lattice at half filling. The calculation reveals two discontinuities in the double occupancy with increasing the repulsive Hubbard interaction U at $U_{c1} \sim 7.55t$ and $U_{c2} \sim 9.65t$ (t being the hopping integral), indicating that there are three phases separated by first order transitions. The absence of any singularity in physical quantities for $0 \leq U < U_{c1}$ implies that this phase corresponds to a metallic phase. The local spin density induced by an applied pinning magnetic field for $U > U_{c2}$ exhibits a three sublattice feature, which is compatible with the 120° Néel ordered state realized in the limit of $U \rightarrow \infty$. For $U_{c1} < U < U_{c2}$, a response to the applied pinning magnetic field is comparable to that in the metallic phase but a relatively large spin correlation length is found with neither valence bond nor chiral magnetic order, suggesting a paramagnetic nature which resembles gapless spin liquid.

PACS numbers: 71.10.Fd, 71.20.Rv, 71.30.+h, 75.10.Kt.

There have been accumulating experimental evidences that several organic materials, κ -(BEDT-TTF)₂Cu₂(CN)₃ [1], EtMe₃Sb[Pd(dmit)₂]₂ [2–4], and κ -H₃(Cat-EDT-TTF)₂ [5], forming a quasi two-dimensional (2D) triangular structure exhibit quantum spin liquid (QSL) [6, 7], where any spatial symmetry breaking does not occur even when it is cooled down to zero temperature due to the quantum fluctuation. The realization of QSL against a symmetry-broken Néel ordered state is one of the long standing issues in condensed matter physics [6] since the first proposal of resonating valence bonds (RVB) states by Anderson [8]. It has been considered that one of the key ingredients for the emergence of stable QSL is geometrical frustration [8], which increases quantum fluctuations and thus prevents symmetry breaking. In this context, the spin-1/2 antiferromagnetic Heisenberg model on the triangular lattice had been considered [9]. However, recent numerical studies, including 2D density-matrix renormalization group (2D-DMRG) analysis, have suggested that the ground state of the spatially isotropic model is 120° Néel ordered [10–13].

In addition to the geometrical frustration, other factors have also been considered for stable QSL, such as i) the spatially anisotropic exchange interactions [14], ii) the higher order corrections of exchange interactions [15], and iii) the charge degree of freedom [16]. The later two are captured by the triangular lattice Hubbard model at half electron filling described by the Hamiltonian

$$\mathcal{H} = -t \sum_{\langle i,j \rangle} \sum_{\sigma=\uparrow,\downarrow} (c_{i,\sigma}^\dagger c_{j,\sigma} + \text{h.c.}) + U \sum_i n_{i,\uparrow} n_{i,\downarrow}, \quad (1)$$

where $c_{i,\sigma}$ ($c_{i,\sigma}^\dagger$) represents the annihilation (creation) op-

erator of an electron with spin σ ($=\uparrow, \downarrow$) at site i on the triangular lattice, $n_{i,\sigma} = c_{i,\sigma}^\dagger c_{i,\sigma}$, and the sum $\langle i, j \rangle$ runs over all pairs of nearest-neighbor sites i and j . Indeed, the QSL phase in the organic materials appears next to the metallic phase, indicating that the QSL occurs close to the Mott metal-insulator transition [19–21] and thus the above two factors ii) and iii) seem to be realized. In fact, it has been extensively argued that the triangular lattice Hubbard model is the simplest effective model to describe and understand the metal-insulator transition and the QSL phase in the organic materials [22].

Elucidating the ground state phase diagram of the triangular lattice Hubbard model at half filling is a challenge for numerical techniques in strongly correlated electron systems. Various numerical methods [23–42] have been applied so far, but the results are, nevertheless, controversial. The exact diagonalization techniques [23–25], the variational cluster approximation (VCA) [26, 27], the path-integral renormalization group (PIRG) method [28, 29], as well as the recently proposed ladder dual-Fermion approach [30] have suggested that there exist three phases in the ground state phase diagram with increasing U/t , i.e., a metallic phase, a non-magnetic insulating phase, and the 120° Néel ordered insulating phase. This is also supported by the numerical analysis of an effective strong coupling spin model [31]. On the other hand, the variational Monte Carlo methods [39–42] have suggested the absence of the nonmagnetic insulating phase. Besides the presence or absence of the intermediate insulating phase, the critical U_c/t for the metal-insulator transition significantly varies among

different methods [25].

Recently, the 2D-DMRG method was applied to various 2D strongly correlated quantum systems [43–58], although the DMRG method is best performed for one-dimensional gapful systems [59–62]. This is because the calculations with keeping large enough number of adapted density-matrix eigenstates to guarantee the desired numerical accuracy became possible within reasonable computational resources specially for 2D spin-1/2 Heisenberg models [43].

Here, we employ the 2D-DMRG method to examine the ground state phase diagram of the repulsive Hubbard model on the triangular lattice at half electron filling. Our calculation reveals two discontinuities in the double occupancy of electrons with increasing U/t , e.g., at $U_{c1} \sim 7.55t$ and $U_{c2} \sim 9.65t$ for a 36-site cluster, strongly indicating that there are three phases separated by first order transitions at U_{c1} and U_{c2} . The spin oscillation pattern for $U > U_{c2}$ under a pinning magnetic field exhibits a three sublattice feature, compatible with the 120° Néel ordered state. The spatial distribution of the nearest-neighbor spin correlation is found to be quite different among the three phases. The suppression of oscillatory behavior in the intermediate phase at $U_{c1} < U < U_{c2}$ suggests this phase in neither bond order nor valence bond solid. In addition, the spin correlation length in the intermediate phase is found to be larger than that for $U < U_{c1}$ and smaller than that for $U > U_{c2}$. However, the response to a pinning magnetic field in the intermediate phase is rather comparable to that in the paramagnetic metallic state. These features imply that the ground state in the intermediate phase resembles gapless spin liquid [22, 63].

Although we mainly focus on a 36-site cluster with open (periodic) boundary conditions in x -direction (y -direction), as schematically shown in Fig. 1, the results for other clusters are qualitatively the same [64]. Throughout the study, we set the z component of total spin to be zero and keep up to $m = 14000$ density-matrix eigenstates, for which the typical orders of the discarded weight are 2×10^{-5} for $U = 6t$, 3×10^{-6} for $U = 8.5t$, and 7×10^{-7} for $U = 11t$ [65].

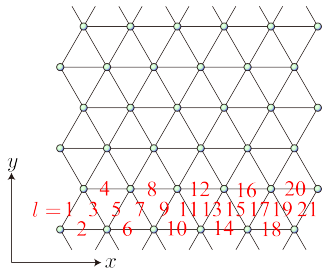


Figure 1. (color online) A 36-site cluster studied here. Open (periodic) boundary conditions are imposed in x -direction (y -direction). The indexing of bonds ($l = 1, 2, \dots, 21$) is also indicated.

We first discuss the U/t dependence of the ground state energy and double occupancy. Figures 2(a) and 2(b) show the ground state energy per site $\varepsilon_0 = \langle \psi_0 | \mathcal{H} | \psi_0 \rangle / N$ and the site average of the double occupancy $n_d = \sum_i \langle \psi_0 | n_{i,\uparrow} n_{i,\downarrow} | \psi_0 \rangle / N$, where $|\psi_0\rangle$ is the ground state obtained by the 2D-DMRG calculation and N is the number of sites. As shown in Figs. 2(a) and 2(b), a reasonable convergency is achieved for these quantities with $m = 14000$ [64]. We also find in Fig. 2(b) that there exist two discontinuities in the double occupancy. It should be noted that ε_0 and n_d are related via $n_d = \partial \varepsilon_0 / \partial U$. We have numerically verified this relation, supporting the satisfactory convergence of our results with $m = 14000$.

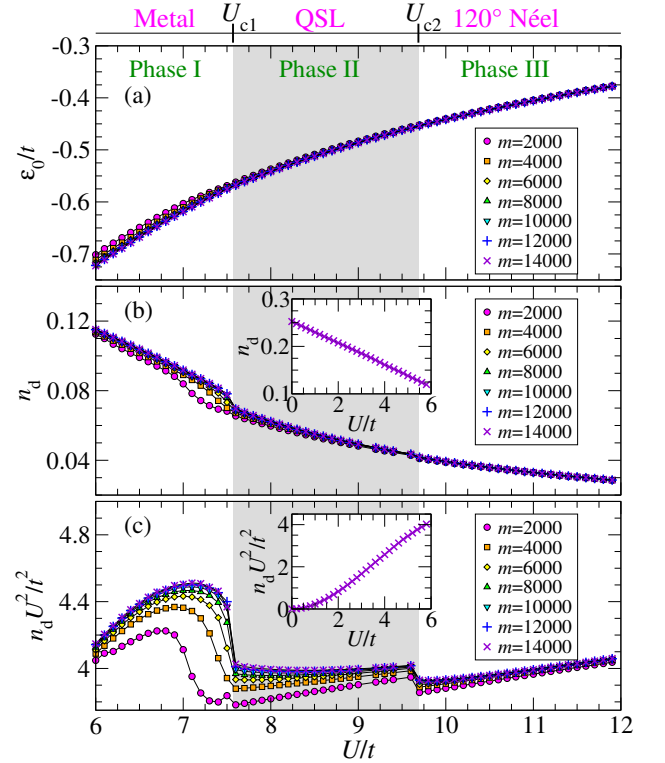


Figure 2. (color online) (a) Ground state energy per site ε_0 , (b) double occupancy n_d , and (c) $n_d U^2$ for different number m of density-matrix eigenstates kept. Insets in (b) and (c) show the results for small values of U with $m = 14000$. The intermediate phase (phase II) at $U_{c1} < U < U_{c2}$ is indicated by gray shade. The ground state phase diagram is shown schematically in the top panel, where QSL denotes quantum spin liquid.

As shown in Fig. 2(c), the discontinuities in the double occupancy are most apparent when $n_d U^2$ is plotted. The first discontinuity occurs at $U_{c1}/t = 7.55 \pm 0.05$ and the second one is located at $U_{c2}/t = 9.65 \pm 0.05$. These discontinuities in $n_d U^2$ become sharper with increasing m , indicating the nature of first order transition. We also find in the insets of Figs. 2(b) and 2(c) that there is no additional discontinuity for $0 \leq U \leq 6t$. Therefore, we conclude that there exist two first order transi-

tions separating three phases. We find that these three phases appear also in a different cluster with the critical interactions still showing some dependence on the cluster shape [64]. In the following, we call the three regions phases I, II, and III, as indicated in Fig. 2.

Let us now compare our results with the previous studies. Since it includes the noninteracting limit with $U = 0$, phase I is regarded as the metallic phase. The exact diagonalization analysis of a 16-site cluster using a finite temperature Lanczos method has found that the metal-insulator transition occurs at $U_c/t = 7.5 \pm 0.5$ [25]. The metal-insulator transition is also found at $U_c/t \sim 7.4 \pm 0.1$ for clusters up to 36 sites by the PIRG method [29]. These U_c values are rather similar to U_{c1} in our calculations. On the other hand, the metal-insulator transition found by the VCA is at $U_c/t \sim 6.3 - 6.7$ [26, 27], which is slightly smaller than U_{c1} . This is probably due to smaller clusters used in these VCA calculations, which tend to enhance an insulating phase.

The analysis based on the strong coupling expansion of the triangular lattice Hubbard model for clusters up to 36 sites [31] finds that the phase transition from the 120° Néel ordered phase to an insulating QSL phase occurs at $U_c \sim 10t$, which is close to U_{c2} obtained in our calculation. The intermediate insulating phase with $U_{c2} = 9.2t \pm 0.3t$ is also reported in the PIRG calculations [29]. Based on the comparison with these previous studies, phases II and III found in our calculations should correspond to a QSL phase and the 120° Néel ordered phase, respectively. We now examine the nature of these phases.

Let us first explore a possible magnetic order by applying a pinning magnetic field along the z -direction at a single site located at the edge of the cluster (see Fig. 3). The results for the local spin density $S_i^z = \langle \psi_0 | S_i^z | \psi_0 \rangle$ with $S_i^z = (n_{i,\uparrow} - n_{i,\downarrow})/2$ are summarized in Fig. 3 [66]. As shown in Fig. 3(c), the local spin density for $U = 11t$ in phase III exhibits essentially a three sublattice pattern, compatible with the 120° Néel order, except that there exists a domain wall at the center of the cluster running along y -direction. Note that, in the presence of the pinning magnetic field, a similar domain wall is found in the spin-1/2 antiferromagnetic Heisenberg model [64], where the ground state is 120° Néel ordered [10–13]. In contrast, as shown in Figs. 3(a) and (b), the local spin densities for $U = 6t$ in phase I and $U = 8.5t$ in phase II are less affected by the pinning magnetic field, indicating the absence of long-range magnetic order.

Next, we calculate the spin correlation $S_{i,j} = \langle \psi_0 | S_i^z S_j^z | \psi_0 \rangle$ between a reference site j located at the center of the cluster and other sites i . The representative results for the three different phases are shown in Fig. 4. Fig. 4(c) clearly shows that $S_{i,j}$ for $U = 11t$ in phase III exhibits a three sublattice pattern, compatible with the 120° Néel order. On the other hand, $S_{i,j}$ in phases I and II does not show such a three sublattice pattern [Figs. 4(a) and 4(b)], strongly suggesting that these phases are not 120° Néel ordered.

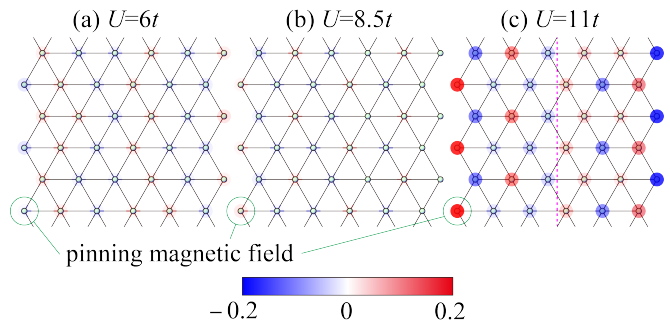


Figure 3. (color online) Local spin density S_i^z for (a) $U = 6t$, (b) $U = 8.5t$, and (c) $U = 11t$ when a pinning magnetic field $h = 0.005t$ is applied along z -direction at a single site located at the edge of the cluster (indicated by a green open circle). Dashed line in (c) indicates a domain wall separating the cluster into two pieces, each of which exhibits a three sublattice pattern, expected for the 120° Néel order. Note that the z component of total spin is kept zero, i.e., $\sum_{i=1}^N S_i^z = 0$, in the calculations.

We can notice however in Fig. 4 that the intensity of $S_{i,j}$ between distant sites for $U = 8.5t$ is comparable to that for $U = 11t$, indicating the relatively long spin correlation in phase II. For a quantitative comparison, we estimate the correlation length ξ via $\xi = 2\sqrt{\sum_i |S_{i,j} \mathbf{r}_{i,j}|^2 / \sum_i |S_{i,j}|^2}$, where $\mathbf{r}_{i,j} = \mathbf{r}_i - \mathbf{r}_j$ and \mathbf{r}_i is the position vector of site i . As shown in Fig. 4, we find that ξ for $U = 8.5t$ is shorter than that for $U = 11t$ where ξ diverges in the thermodynamic limit, but is longer than that for $U = 6t$ where the spin correlation decays algebraically. The rather long range spin correlation in phase II should be contrasted with the exponential decay of spin correlation expected in gapped QSL. Recalling also the result of the response to the pinning magnetic field, the ground state in phase II resembles gapless QSL. We should note however that the spin structure factor displays no Fermi surface singularity [64] and thus the ground state in phase II is neither compatible with spinon Fermi sea [15] nor with spin Bose metal [67].

We also calculate the nearest-neighbor spin correlations $S_{\langle i,j \rangle}$ for all nearest-neighbor sites, and the representative results for the three different phases are shown in Fig. 5. For better quantitative comparison, we show in Fig. 5(d) $S(l) = S_{\langle i,j \rangle}$ along x -direction, where the bond index l connecting sites i and j is denoted in Fig. 1. It is clearly seen in Fig. 5(d) that $S(l)$ for $U = 11t$ is rather enhanced at $l = 4n - 3$ and suppressed at $l = 4n - 1$ for $n = 1, 2, 3, \dots$. More interestingly, the oscillations in $S(l)$ for $U = 8.5t$ are smallest, especially around the center of the cluster. Note that spatial variation of $S(l)$ is an indication of spatial symmetry breaking, e.g., valence bond solid, or a tendency for it, and that in our case the spatial variations are induced by open boundary conditions in x -direction. The strong suppression of oscillations in phase II is therefore a strong indication of the absence of the valence bond solid and also other pos-

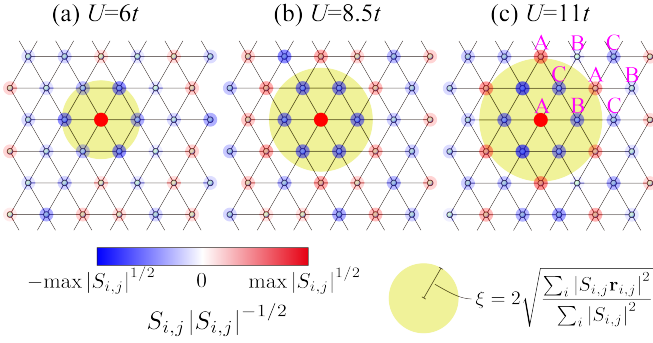


Figure 4. (color online) Spin correlation function $S_{i,j}/\sqrt{|S_{i,j}|}$ between a reference site j at the center of the cluster (indicated by a red circle) and other sites for (a) $U = 6t$, (b) $U = 8.5t$, and (c) $U = 11t$. Here, $\max |S_{i,j}|^{1/2}$ represents the maximum value of $|S_{i,j}|^{1/2}$ for each U . Yellow-green circle indicates the correlation length ξ . A three sublattice pattern expected for the 120° Néel order is indicated in (c) by “A”, “B”, and “C”, where $S_{i,j}$ shows ferromagnetic (antiferromagnetic) correlation if sites i and j belong to the same (different) sublattice.

sible spatial symmetry breakings. In Supplemental Material [64], we calculate the hopping amplitude between nearest-neighbor sites, exhibiting the similar oscillation pattern, which also implies the absence of spatial symmetry breakings such as bond order. These results further support phase II being a QSL.

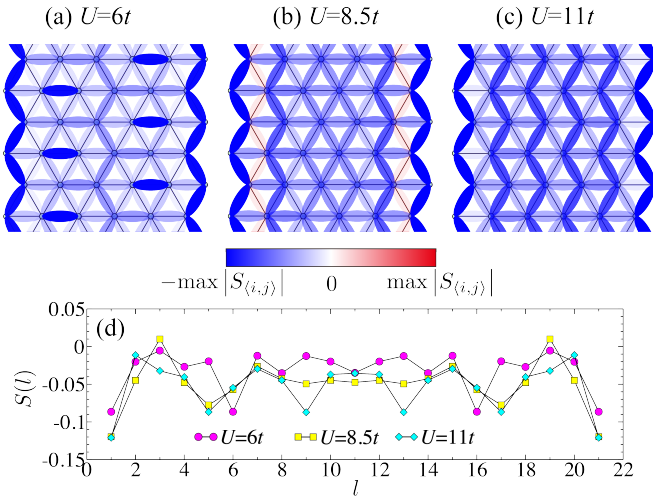


Figure 5. (color online) Intensity plot of nearest-neighbor spin correlation $S_{i,j}$ for (a) $U = 6t$, (b) $U = 8.5t$, and (c) $U = 11t$. Here, $\max |S_{i,j}|$ represents the maximum value of $|S_{i,j}|$ for each U . (d) $S(l) = S_{i,j}$ along x -direction, where the bond index l connecting sites i and j is shown in Fig. 1.

Let us now compare the nature of the ground state in phase II with the Z_2 spin liquid ground state of the spin-1/2 antiferromagnetic Heisenberg model on the triangu-

lar lattice with the next nearest-neighbor exchange interaction, recently reported in Refs. 56 and 57. The cluster used here (Fig. 1) is an odd cylinder [56, 57] with odd number of sites in the one dimensional unit cell. Therefore, according to the Lieb-Schultz-Mattis theorem [68], the ground state for this cluster is degenerate if the excitation gap is finite as in the case for the Z_2 spin liquid. Reflecting this degeneracy, the spatial distribution of the nearest-neighbor spin correlation $S_{i,j}$ exhibits the strong alternating oscillation, induced by open boundary conditions along x -direction [56, 57]. Although the similar oscillation pattern is found in phase III and around the edge of the cluster in phase II, the central region of the cluster in phase II does not show such feature (see Fig. 5). Since the cluster used here is much smaller than those in Refs. 56 and 57, the more detail analysis using larger clusters is highly desirable in order to determine the nature of the ground state in phase II and, in particular, to address experimental observation of gapless QSL in $\text{EtMe}_3\text{Sb}[\text{Pd}(\text{dmit})_2]_2$ [3]. We have also calculated the chiral correlation function and found that the chiral spin liquid [50] is unlikely in phase II [64].

Finally, we emphasize a rather small discontinuity Δn_d (~ 0.007) in the double occupancy found at the metal-insulator transition U_{c1} , which is in sharp contrast to the previous studies using other approaches, where Δn_d is typically much larger (from 0.02 to 0.06), and is even qualitatively different from the continuous transition discussed in Refs. 69 and 70. Smallness of the jump might be the origin of the controversy about the order of the transition. We note, however, that the discontinuity Δn_d corresponds to the interaction (or equivalently kinetic) energy jump of $U_{c1}\Delta n_d \sim 0.05t$, giving ~ 25 K for the organic materials with $t \sim 50$ meV [25], which nicely compares with the temperature where the first order transition line ends in the phase diagram of the organic materials [20].

In summary, we have performed large scale 2D-DRMG calculations, using up to $m = 14000$ density-matrix eigenstates, to examine the ground state phase diagram of the Hubbard model on the triangular lattice at half filling. We have shown that the convergence of our results is well controlled and, therefore, our results can be regarded as the most accurate and unbiased results available at a moment, apart from the small cluster shape and size dependence. We have found two first order transitions separating the three different phases, which include a gapless QSL like phase in the intermediate region. Further properties of this phase, such as the nature of its excitations, remain to be firmly examined since that would greatly improve our understanding of spin liquids in general as well as of the organic materials in particular.

The authors are grateful to S. Nishimoto and T. Li for valuable discussion. This work has been supported by Grant-in-Aid for Scientific Research from the Japan Society for the Promotion of Science (JSPS) (Grant Nos. 24740269 and 26287079), MEXT HPCI Strategic Programs for Innovative Research (SPIRE) (Grant Nos. hp120137, hp140128, hp150112, and hp160122),

and Slovenian Research Agency (Z1-5442), and in part by RIKEN Molecular Systems and RIKEN iTHES Project. T. T. and J. K. acknowledge the visiting program for young researchers at Yukawa Institute for Theoretical Physics, Kyoto University. The computation has been

performed using the RIKEN Cluster of Clusters (RICC), the RIKEN supercomputer system (HOKUSAI Great-Wave), and the K computer at RIKEN Advanced Institute for Computational Science (AICS).

-
- [1] Y. Shimizu, K. Miyagawa, K. Kanoda, M. Maesato, and G. Saito, *Spin liquid state in an organic Mott insulator with a triangular Lattice*, *Phys. Rev. Lett.* **91**, 107001 (2003).
 - [2] T. Itou, A. Oyamada, S. Maegawa, M. Tamura, and R. Kato, *Spin-liquid state in an organic spin-1/2 system on a triangular lattice*, *J. Phys.: Condens. Matter* **19**, 145247 (2007).
 - [3] M. Yamashita, N. Nakata, Y. Senshu, M. Nagata, H. M. Yamamoto, R. Kato, T. Shibauchi, Y. Matsuda, *Highly mobile gapless excitations in a two-dimensional candidate quantum spin liquid*, *Science* **328**, 1246 (2010).
 - [4] S. Yamashita, T. Yamamoto, Y. Nakazawa, M. Tamura, and R. Kato, *Gapless spin liquid of an organic triangular compound evidenced by thermodynamic measurements*, *Nat. Commun.* **2**, 275 (2011).
 - [5] T. Isono, H. Kamo, A. Ueda, K. Takahashi, M. Kimata, H. Tajima, S. Tsuchiya, T. Terashima, S. Uji, and H. Mori, *Gapless quantum spin liquid in an organic spin-1/2 triangular-lattice κ -H₃(Cat-EDT-TTF)₂*, *Phys. Rev. Lett.* **112**, 177201 (2014).
 - [6] P. A. Lee, *An end to the drought of quantum spin liquids*, *Science* **321**, 1306 (2008).
 - [7] L. Balents, *Spin liquids in frustrated magnets*, *Nature* **464**, 199 (2010).
 - [8] P. W. Anderson, *Resonating valence bonds: A new kind of insulator?*, *Mater. Res. Bull.* **8**, 153 (1973).
 - [9] P. Fazekas and P. W. Anderson, *On the ground state properties of the anisotropic triangular antiferromagnet*, *Phil. Mag.* **30**, 423 (1974).
 - [10] B. Bernu, P. Lecheminant, C. Lhuillier, and L. Pierre, *Exact spectra, spin susceptibilities, and order parameter of the quantum Heisenberg antiferromagnet on the triangular lattice*, *Phys. Rev. B* **50**, 10048 (1994).
 - [11] L. Capriotti, A. E. Trumper, and S. Sorella, *Long-range Néel order in the triangular Heisenberg model*, *Phys. Rev. Lett.* **82**, 3899 (1999).
 - [12] W. Zheng, J. O. Fjærestad, R. R. P. Singh, R. H. McKenzie, and R. Coldea, *Excitation spectra of the spin-1/2 triangular-lattice Heisenberg antiferromagnet*, *Phys. Rev. B* **74**, 224420 (2006).
 - [13] S. R. White and A. L. Chernyshev, *Neél order in square and triangular lattice Heisenberg models*, *Phys. Rev. Lett.* **99**, 127004 (2007).
 - [14] S. Yunoki and S. Sorella, *Two spin liquid phases in the spatially anisotropic triangular Heisenberg model*, *Phys. Rev. B* **74**, 014408 (2006).
 - [15] O. I. Motrunich, *Variational study of triangular lattice spin-1/2 model with ring exchanges and spin liquid state in κ -(ET)₂Cu₂(CN)₃*, *Phys. Rev. B* **72**, 045105 (2005).
 - [16] In the context of the organic materials, other factors, e.g., the intra-dimer degree of freedom [17, 18], the electron-lattice coupling, and the spin-orbit coupling [7], have also been discussed.
 - [17] C. Hotta, *Quantum electric dipoles in spin-liquid dimer Mott insulator κ -ET₂Cu₂(CN)₃*, *Phys. Rev. B* **82**, 241104 (2010).
 - [18] M. Naka and S. Ishihara, *Electronic ferroelectricity in a dimer Mott insulator*, *J. Phys. Soc. Jpn.* **79**, 063707 (2010).
 - [19] Y. Kurosaki, Y. Shimizu, K. Miyagawa, K. Kanoda, and G. Saito, *Mott transition from a spin liquid to a Fermi liquid in the spin-frustrated organic conductor κ -(ET)₂Cu₂(CN)₃*, *Phys. Rev. Lett.* **95**, 177001 (2005).
 - [20] T. Furukawa, K. Miyagawa, H. Taniguchi, R. Kato, and K. Kanoda, *Quantum criticality of Mott transition in organic materials*, *Nature Phys.* **11**, 221 (2015).
 - [21] H. C. Kandpal, I. Opahle, Y.-Z. Zhang, H. O. Jeschke, and R. Valentí, *Revision of model parameters for κ -type charge transfer salts: An ab initio study*, *Phys. Rev. Lett.* **103**, 067004 (2009).
 - [22] B. J. Powell and R. H. McKenzie, *Quantum frustration in organic Mott insulators: from spin liquids to unconventional superconductors*, *Rep. Prog. Phys.* **74**, 056501 (2011).
 - [23] T. Koretsune, Y. Motome, and A. Furusaki, *Exact diagonalization study of Mott transition in the Hubbard model on an anisotropic triangular lattice*, *J. Phys. Soc. Jpn.* **76**, 074719 (2007).
 - [24] R. T. Clay, H. Li, and S. Mazumdar, *Absence of superconductivity in the half-filled band Hubbard model on the anisotropic triangular lattice*, *Phys. Rev. Lett.* **101**, 166403 (2008).
 - [25] J. Kokalj and R. H. McKenzie, *Thermodynamics of a bad metal-Mott insulator transition in the presence of frustration*, *Phys. Rev. Lett.* **110**, 206402 (2013).
 - [26] P. Sahebsara and D. Sénéchal, *Hubbard model on the triangular lattice: Spiral order and spin liquid*, *Phys. Rev. Lett.* **100**, 136402 (2008).
 - [27] A. Yamada, *Magnetic properties and Mott transition in the Hubbard model on the anisotropic triangular lattice*, *Phys. Rev. B* **89**, 195108 (2014).
 - [28] H. Morita, S. Watanabe, and M. Imada, *Nonmagnetic insulating states near the Mott transitions on lattice with geometrical frustration and implications for κ -(ET)₂Cu₂(CN)₃*, *J. Phys. Soc. Jpn.* **71**, 2109 (2002).
 - [29] T. Yoshioka, A. Koga, and N. Kawakami, *Quantum phase transition in the Hubbard model on a triangular lattice*, *Phys. Rev. Lett.* **103**, 036401 (2009).
 - [30] G. Li, A. N. Antipov, A. N. Rubtsov, S. Kirchner, and W. Hanke, *Competing phases of the Hubbard model on a triangular lattice: Insights from the entropy*, *Phys. Rev. B* **89**, 161118(R) (2014).
 - [31] H. Y. Yang, A. M. Läuchli, F. Mila, and K. P. Schmidt, *Effective spin model for the spin-liquid phase of the Hubbard model on the triangular lattice*, *Phys. Rev. Lett.* **105**, 267204 (2010).
 - [32] B. Kyung and A.-M. S. Tremblay, *Mott transition, an-*

- tiferromagnetism, and *d*-wave superconductivity in two-dimensional organic conductors, *Phys. Rev. Lett.* **97**, 046402 (2006).
- [33] A. Liebsch, H. Ishida, and J. Merino, *Mott transition in two-dimensional frustrated compounds*, *Phys. Rev. B* **79**, 195108 (2009).
- [34] D. Galanakis, T. D. Stanescu, and P. Phillips, *Mott transition on a triangular lattice*, *Phys. Rev. B* **79**, 115116 (2009).
- [35] T. Ohashi, T. Momoi, H. Tsunetsugu, and N. Kawakami, *Finite temperature Mott transition in Hubbard model on anisotropic triangular lattice*, *Phys. Rev. Lett.* **100**, 076402 (2008).
- [36] T. Sato, K. Hattori, and H. Tsunetsugu, *Transport criticality at the Mott transition in a triangular-lattice Hubbard model*, *Phys. Rev. B* **86**, 235137 (2012).
- [37] H. Lee, G. Li, and H. Monien, *Hubbard model on the triangular lattice using dynamical cluster approximation and dual fermion methods*, *Phys. Rev. B* **78**, 205117 (2008).
- [38] H. T. Dang, X. Y. Xu, K.-S. Chen, Z. Y. Meng, and S. Wessel, *Mott transition in the triangular lattice Hubbard model: A dynamical cluster approximation study*, *Phys. Rev. B* **91**, 155101 (2015).
- [39] T. Watanabe, H. Yokoyama, Y. Tanaka, and J. Inoue, *Superconductivity and a Mott transition in a Hubbard model on an anisotropic triangular lattice*, *J. Phys. Soc. Jpn.* **75**, 074707 (2006).
- [40] T. Watanabe, H. Yokoyama, Y. Tanaka, and J. Inoue, *Predominant magnetic states in the Hubbard model on anisotropic triangular lattices*, *Phys. Rev. B* **77**, 214505 (2008).
- [41] L. F. Tocchio, H. Feldner, F. Becca, R. Valentí, and C. Gros, *Spin-liquid versus spiral-order phases in the anisotropic triangular lattice*, *Phys. Rev. B* **87**, 035143 (2013).
- [42] L. F. Tocchio, C. Gros, R. Valentí, and F. Becca, *One-dimensional spin liquid, collinear, and spiral phases from uncoupled chains to the triangular lattice*, *Phys. Rev. B* **89**, 235107 (2014).
- [43] E. M. Stoudenmire and S. R. White, *Studying two-dimensional systems with the density matrix renormalization group*, *Annual. Rev. Condens. Matter Phys.* **3**, 111 (2012).
- [44] H.-C. Jiang, H. Yao, and L. Balents, *Spin liquid ground state of the spin-1/2 square J_1 - J_2 Heisenberg model*, *Phys. Rev. B* **86**, 024424 (2012).
- [45] S.-S. Gong, W. Zhu, D. N. Sheng, O. I. Motrunich, and M. P. A. Fisher, *Plaquette ordered phase and quantum phase diagram in the spin-1/2 J_1 - J_2 square Heisenberg model*, *Phys. Rev. Lett.* **113**, 027201 (2014).
- [46] S. Yan, D. A. Huse, and S. R. White, *Spin-liquid ground state of the $S = 1/2$ kagome Heisenberg antiferromagnet*, *Science* **332**, 1173 (2011).
- [47] H.-C. Jiang, Z. Wang, and L. Balents, *Identifying topological order by entanglement entropy*, *Nat. Phys.* **8**, 902 (2012).
- [48] S. Dendbrock, I. P. McCulloch, and U. Schollwöck, *Nature of the spin-liquid ground state of the $S = 1/2$ Heisenberg model on the kagome lattice*, *Phys. Rev. Lett.* **109**, 067201 (2012).
- [49] S. Nishimoto, N. Shibata, and C. Hotta, *Controlling frustrated liquids and solids with an applied field in a kagome Heisenberg antiferromagnet*, *Nat. Commun.* **4**, 2287 (2013).
- [50] S.-S. Gong, W. Zhu, and D. N. Sheng, *Emergent chiral spin liquid: fractional quantum Hall effect in a kagome Heisenberg model*, *Sci. Rep.* **4**, 6317 (2014).
- [51] S.-S. Gong, W. Zhu, L. Balents, and D. N. Sheng, *Global phase diagram of competing ordered and quantum spin-liquid phases on the kagome lattice*, *Phys. Rev. B* **91**, 075112 (2015).
- [52] R. Ganesh, S. Nishimoto, and J. van den Brink, *Plaquette resonating valence bond state in a frustrated honeycomb antiferromagnet*, *Phys. Rev. B* **87**, 054413 (2013).
- [53] R. Ganesh, J. van den Brink, and S. Nishimoto, *Deconfined criticality in the frustrated Heisenberg honeycomb antiferromagnet*, *Phys. Rev. Lett.* **110**, 127203 (2013).
- [54] S. Shinjo, S. Sota, and T. Tohyama, *Density-matrix renormalization group study of the extended Kitaev-Heisenberg model*, *Phys. Rev. B* **91**, 054401 (2015).
- [55] T. Tohyama, K. Tsutsui, M. Mori, S. Sota, and S. Yunoki, *Enhanced charge excitations in electron-doped cuprates by resonant inelastic x-ray scattering*, *Phys. Rev. B* **92**, 014515 (2015).
- [56] Z. Zhu and S. R. White, *Spin liquid phase of the $S = 1/2$ J_1 - J_2 Heisenberg model on the triangular lattice*, *Phys. Rev. B* **92**, 041105(R) (2015).
- [57] W.-J. Hu, S.-S. Gong, W. Zhu, and D. N. Sheng, *Competing spin liquid states in the spin-1/2 Heisenberg model on triangular lattice*, *Phys. Rev. B* **92**, 140403(R) (2015).
- [58] K. Shinjo, S. Sota, S. Yunoki, K. Totsuka, T. Tohyama, *Density-matrix renormalization group study of Kitaev-Heisenberg model on the triangular lattice*, *arXiv:1512.02334*.
- [59] S. R. White, *Density matrix formulation for quantum renormalization groups*, *Phys. Rev. Lett.* **69**, 2863 (1992).
- [60] S. R. White, *Density-matrix algorithms for quantum renormalization groups*, *Phys. Rev. B* **48**, 10345 (1993).
- [61] U. Schollwöck, *The density-matrix renormalization group*, *Rev. Mod. Phys.* **77**, 259 (2005).
- [62] K. Hallberg, *New trends in density matrix renormalization*, *Adv. Phys.* **55**, 477 (2010).
- [63] B. Normand, *Frontiers in frustrated magnetism*, *Contemp. Phys.* **50**, 533 (2009).
- [64] See Supplemental Material for double occupancy, energy convergence, spin response, spin structure factor, hopping amplitude, and chiral correlation function.
- [65] The discarded weight δ is defined as $\delta = 1 - \sum_{\mu=1}^m \lambda_{\mu}$, where λ_{μ} is the μ -th largest eigenvalue of the reduced density matrix.
- [66] Note that the local spin density S_i^z is zero in the absence of the pinning magnetic field.
- [67] M. S. Block, D. N. Sheng, O. I. Motrunich, and M. P. A. Fisher, *Spin Bose-Metal and Valence Bond Solid Phases in a Spin-1/2 Model with Ring Exchanges on a Four-Leg Triangular Ladder*, *Phys. Rev. Lett.* **106**, 157202 (2011).
- [68] E. H. Lieb, T. D. Schultz, and D. C. Mattis, *Two soluble models of an antiferromagnetic chain*, *Ann. Phys. (N.Y.)* **16**, 407 (1961).
- [69] T. Senthil, *Theory of a continuous Mott transition in two dimensions*, *Phys. Rev. B* **78**, 045109 (2008).
- [70] R. V. Mishmash, I. González, R. G. Melko, O. I. Motrunich, and M. P. A. Fisher, *Continuous Mott transition between a metal and a quantum spin liquid*, *Phys. Rev. B* **91**, 235140 (2015).

A: Supplemental Material

1. Double occupancy

Here, we examine the U dependence of double occupancy for different clusters. Following Refs. 1 and 2, we classify different clusters using $\text{XC}n$ ($\text{YC}n$) for which the bond direction of a cluster is parallel to x -direction (y -direction), as shown in Fig. S1, and n in $\text{XC}n$ ($\text{YC}n$) represents the number of bonds in zigzag (vertical) y -direction.

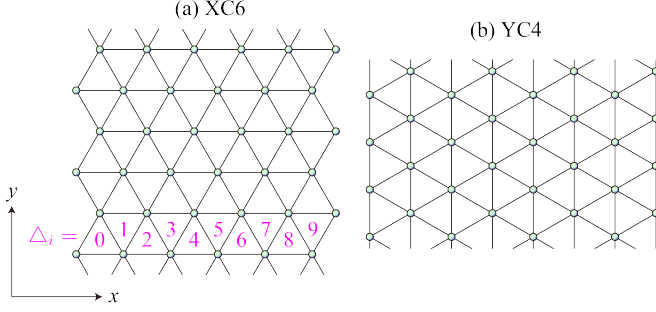


Figure S1. (color online) (a) $\text{XC}6$ and (b) $\text{YC}4$ clusters. Open (periodic) boundary conditions are imposed in x -direction (y -direction). The total number N of sites is 36 for $\text{XC}6$ and 32 for $\text{YC}4$. The cluster studied in the main text is $\text{XC}6$. The indexing of elementary triangles, $\Delta_i = 0, 1, 2, \dots, 9$, is indicated in (a).

Figure S2 shows the ground state energy per site ϵ_0 and the double occupancy n_d for different clusters. It is apparent in Fig. S2(c) that the double occupancy exhibits two discontinuities with increasing U/t for both clusters, although the critical U still shows some dependence on the cluster shape.

2. Energy convergence

Figure S3 shows the convergence of the ground state energy as a function of the discarded weight δ_m defined as

$$\delta_m = 1 - \sum_{\alpha=1}^m \lambda_{\alpha}, \quad (\text{s1})$$

where λ_{α} is the α -th largest eigenvalue of the reduced density matrix. As shown in Fig. S3, we find that the ground state energy for $m \geq 10000$ scales linearly with δ_m , implying that the convergence of our calculations is well controlled.

3. Response to a pinning magnetic field

Figure S4 shows the local spin density $S_i^z = \langle \psi_0 | \mathcal{S}_i^z | \psi_0 \rangle$ with $\mathcal{S}_i^z = (n_{i,\uparrow} - n_{i,\downarrow})/2$ calculated in the presence of a

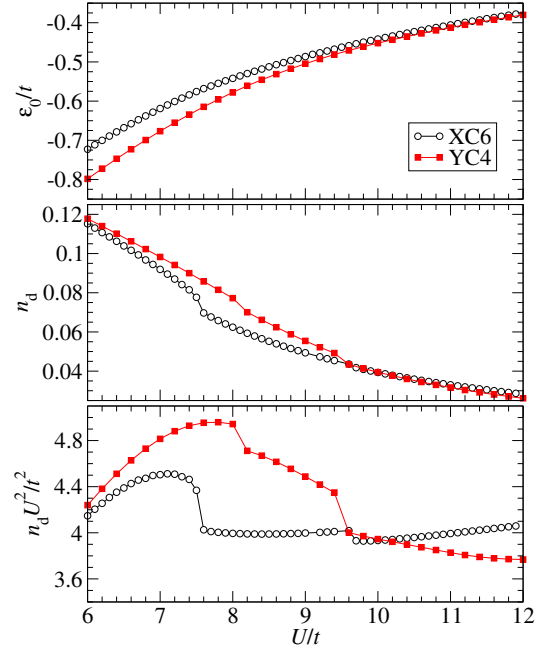


Figure S2. (color online) (a) Ground state energy per site ϵ_0 , (b) double occupancy n_d , and (c) $n_d U^2$ for two different clusters $\text{XC}6$ and $\text{YC}4$ (see Fig. S1). The number m of density-matrix eigenstates kept is 14000 (10000) for the $\text{XC}6$ ($\text{YC}4$) cluster.

pinning magnetic field that is applied at a single site of the $\text{XC}6$ cluster, where the z component of total spin is kept zero, i.e., $\sum_i S_i^z = 0$. It is apparent in Fig. S4 that S_i^z for $U = 11t$ in phase III exhibits essentially the same pattern, including the domain wall structure, as that for the spin-1/2 antiferromagnetic Heisenberg model on the triangular lattice with the nearest-neighbor exchange interaction J , where the ground state is 120° Néel ordered. This is a strong evidence that the ground state in phase III is also 120° Néel ordered.

4. Spin excitations

In the main text, we find that the spin correlation length in $S_{i,j} = \langle \psi_0 | \mathcal{S}_i^z \mathcal{S}_j^z | \psi_0 \rangle$ for $U = 8.5t$ in phase II is relatively large as compared with that for $U = 6t$ in phase I (see Fig. 4). On the contrary, we find that the ground states for both $U = 6t$ and $8.5t$ are much less affected by the pinning magnetic field than that for $U = 11t$ (see Fig. 3). These seemingly contradictory features are attributed to the amount of low-lying triplet excitations.

The pinning magnetic field $h_i = h$ applied at site i along z -direction is described by the Hamiltonian

$$\mathcal{H}' = h_i \mathcal{S}_i^z, \quad (\text{s2})$$

where $\mathcal{S}_i^z = (n_{i,\uparrow} - n_{i,\downarrow})/2$. Applying the perturbation theory, the leading correction of the spin density $S_j^z(h_i)$

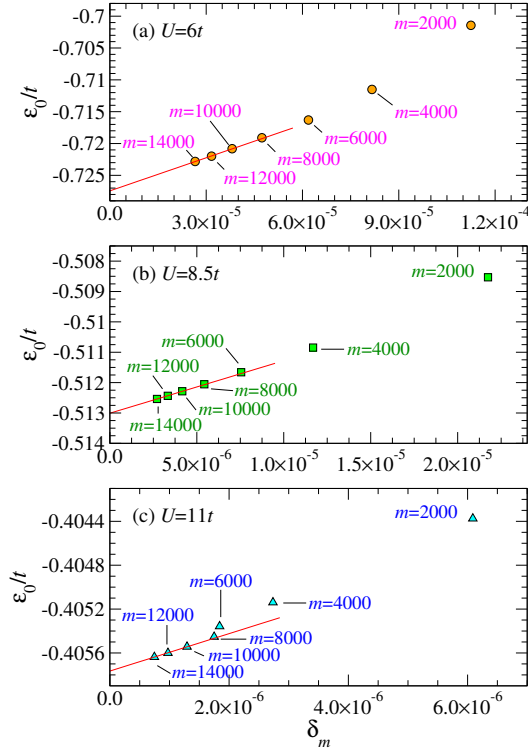


Figure S3. (color online) Ground state energy per site ε_0 as a function of the discarded weight δ_m for (a) $U = 6t$, (b) $U = 8.5t$, and (c) $U = 11t$. The cluster used here is XC6 shown in Fig. S1(a). The number m of kept eigenstates of the reduced density matrix is indicated beside each data point. A red straight line shows a linear fit to the three data points with $m = 10000, 12000$, and 14000 .

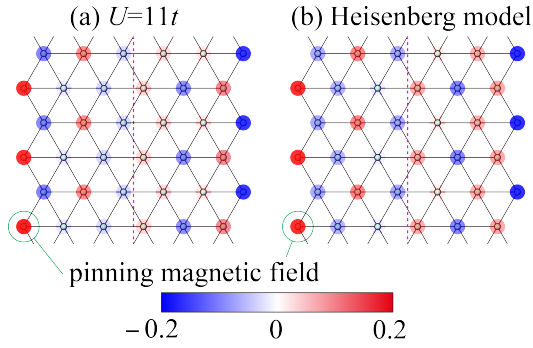


Figure S4. (color online) Local spin density S_i^z for (a) $U = 11t$ and (b) the spin-1/2 antiferromagnetic Heisenberg model with the nearest-neighbor exchange interaction J (i.e., $U \rightarrow \infty$ in the Hubbard model), when a pinning magnetic field [$h = 0.005t$ for (a) and $h = 0.005J$ for (b)] is applied along z -direction at a single site located at the edge of the XC6 cluster (indicated by a green open circle). Dashed vertical line indicates a domain wall separating the cluster into two pieces, each of which exhibits a three sublattice pattern expected for the 120° Néel order.

at site j can be expressed as

$$S_j^z(h_i) \sim h_i \sum_{n \neq 0} \frac{\langle \psi_0 | \mathcal{S}_i^z | \psi_n \rangle \langle \psi_n | \mathcal{S}_j^z | \psi_0 \rangle}{E_0 - E_n}, \quad (\text{s3})$$

where $|\psi_n\rangle$ is the n -th eigenstate of \mathcal{H} (without the pinning magnetic field) with its eigenvalue E_n . Since \mathcal{H} commutes with the total spin operator, the total spin S_{tot} is a good quantum number. We now assume that the ground state $|\psi_0\rangle$ is spin singlet with $S_{\text{tot}} = 0$. Then, the Wigner-Eckert theorem states that the matrix elements in the numerator of Eq. (s3) satisfy

$$\langle \psi_n | \mathcal{S}_j^z | \psi_0 \rangle = \begin{cases} 0 & \text{if } |\psi_n\rangle \notin S_{\text{tot}} = 1 \\ \text{finite} & \text{if } |\psi_n\rangle \in S_{\text{tot}} = 1 \end{cases}, \quad (\text{s4})$$

where $|\psi_n\rangle \in S_{\text{tot}} = 1$ ($|\psi_n\rangle \notin S_{\text{tot}} = 1$) indicates that $|\psi_n\rangle$ belongs (does not belong) to the $S_{\text{tot}} = 1$ subspace. Therefore, the different behavior to the applied pinning magnetic field should be attributed to the amount of the low-lying triplet excitations.

Figure S5 shows the same result as Fig. 3 in the main text but in the logarithmic scale. It clearly shows that the local spin densities S_i^z for $U = 8.5t$ in phase II exhibit comparable amplitude with those for $U = 6t$ in phase I where the ground state is the paramagnetic metal and thus no triplet excitation gap is expected. On the other hand, the local spin densities S_i^z for $U = 8.5t$ are significantly smaller than those for $U = 11t$ in phase III where the ground state is 120° Néel ordered. A similarity to the $U = 6t$ case thus indicates that there exist an extensive amount of gapless spin excitations in phase II expected in the thermodynamic limit.

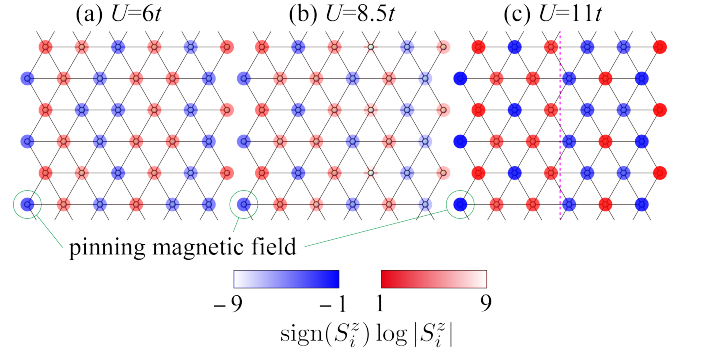


Figure S5. (color online) Local spin density S_i^z in the logarithmic scale for (a) $U = 6t$, (b) $U = 8.5t$, and (c) $U = 11t$, when a pinning magnetic field $h = 0.005t$ is applied along z -direction at a single site located at the edge of the XC6 cluster. Dashed vertical line in (c) indicates a domain wall separating the cluster into two pieces, each of which exhibits a three sublattice pattern, expected for the 120° Néel order. Note that the z component of total spin is kept zero, i.e., $\sum_i S_i^z = 0$, in the calculations.

5. Spin structure factor

The spin structure factor $S(\mathbf{q})$ is the Fourier transform of the real-space spin correlation function $S_{i,j}$ and defined as

$$S(\mathbf{q}) = \sum_i S_{i,j} e^{i\mathbf{q} \cdot (\mathbf{r}_i - \mathbf{r}_j)}, \quad (\text{s5})$$

where \mathbf{r}_i denotes the position vector of site i while site j is a representative site chosen at the central site of the cluster as in Fig. 4. Because of open boundary conditions in x -direction, the wave number \mathbf{q} is not a good quantum number and thus we show the resulting $S(\mathbf{q})$ for arbitrary \mathbf{q} .

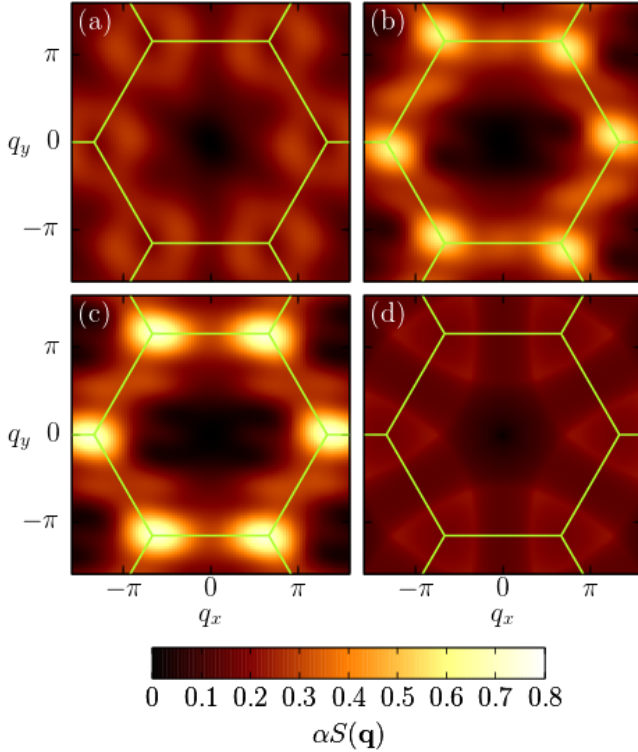


Figure S6. (color online) Intensity plot of spin structure factor $S(\mathbf{q})$ for (a) $U = 6t$, (b) $U = 8.5t$, and (c) $U = 11t$ calculated using the DMRG method for the XC6 cluster, and for (d) $U = 3t$ obtained by the random phase approximation. For clarity, we set $\alpha = 1$ for (a)–(c) and $\alpha = 2$ for (d). The Brillouin zone boundaries are indicated by yellow-green lines.

The representative results for the three different phases are summarized in Figs. S6(a)–(c). We find in Fig. S6(c) that $S(\mathbf{q})$ for $U = 11t$ in phase III displays sharp peaks at $\mathbf{q} = (2\pi/3, 2\pi/\sqrt{3})$ (the K point) and other equivalent \mathbf{q} 's, which is compatible with the 120° Néel ordered state. $S(\mathbf{q})$ for $U = 8.5t$ in phase II shown in Fig. S6(b) also exhibits broad maxima at the K point and other equivalent \mathbf{q} 's, but the peak structure is softened as compared with $S(\mathbf{q})$ for $U = 11t$. In contrast, we find in Fig. S6(a) that

$S(\mathbf{q})$ for $U = 6t$ in phase I shows enhanced intensities forming a ring-like structure around the K point (and other equivalent \mathbf{q} 's), which implies the $2\mathbf{k}_F$ scattering, where \mathbf{k}_F is the Fermi momentum in the noninteracting limit.

In order to better understand $S(\mathbf{q})$ in phases I and II, we calculate $S(\mathbf{q})$ within the random phase approximation (RPA). In RPA, the spin susceptibility is given as

$$\chi(\mathbf{q}, z) = \frac{\chi_0(\mathbf{q}, z)}{1 - U\chi_0(\mathbf{q}, z)}, \quad (\text{s6})$$

where z is the general complex frequency. The susceptibility $\chi_0(\mathbf{q}, z)$ in the noninteracting limit is

$$\chi_0(\mathbf{q}, z) = \frac{1}{N} \sum_{\mathbf{k} \in \text{1st BZ}} \frac{\Theta(-\varepsilon_{\mathbf{k}}) - \Theta(-\varepsilon_{\mathbf{k}+\mathbf{q}})}{z - \varepsilon_{\mathbf{k}} + \varepsilon_{\mathbf{k}+\mathbf{q}}}, \quad (\text{s7})$$

where the sum is taken over the first Brillouin zone (BZ) of the triangular lattice, $\Theta(x)$ is the Heaviside step function, and $\varepsilon_{\mathbf{k}}$ is the noninteracting band dispersion

$$\begin{aligned} \varepsilon_{\mathbf{k}} = & -2t \cos k_x - 2t \cos \left(\frac{k_x}{2} + \frac{\sqrt{3}k_y}{2} \right) \\ & - 2t \cos \left(-\frac{k_x}{2} + \frac{\sqrt{3}k_y}{2} \right) - \mu. \end{aligned} \quad (\text{s8})$$

The chemical potential μ is tuned such that the electron density is 0.5 per spin. We set the chemical potential $\mu = 0.83474569t$ for the calculations in the thermodynamic limit.

From $\chi(\mathbf{q}, z)$ obtained above within RPA, the spin structure factor $S(\mathbf{q})$ is evaluated as

$$\frac{1}{\pi} \int_0^\infty dx \text{Re} \chi(\mathbf{q}, ix) = S(\mathbf{q}). \quad (\text{s9})$$

In deriving the above equation, we have assumed that the z component of total spin is zero and the system is invariant under the global spin flip. $S(\mathbf{q})$ for $U = 3t$ within RPA is shown in Fig. S6(d), where we choose relatively small U because $\chi(\mathbf{q}, 0)$ diverges at $U = 3.7$ – $3.8t$. We find in Fig. S6(d) that $S(\mathbf{q})$ shows a triangular shell-like structure around the K point (and other equivalent \mathbf{q} 's). The ridges of the shells lie exactly along the $2\mathbf{k}_F$ lines and the local minimum in the center of the shell is located at the K point (and other equivalent \mathbf{q} 's). These features are indeed similar to those found in Fig. S6(a) for $U = 6t$.

The spinon Fermi sea state is a kind of gapless spin liquid state and has been considered as a candidate for the ground state of triangular lattice systems [3]. Due to the presence of spinon Fermi surface, $S(\mathbf{q})$ for the spinon Fermi sea state exhibits singularities along the $2\mathbf{k}_F$ lines [4] and is expected to be similar to those shown in Figs. S6(a) and S6(d). However, as shown in Fig. S6(b), we find that $S(\mathbf{q})$ for $U = 8.5t$ in phase II is quite different from those in Figs. S6(a) and S6(d). Therefore, the spinon Fermi sea state is unlikely to be the ground state in phase II.

The similarity of $S(\mathbf{q})$ for $U = 8.5t$ and $U = 11t$ in Fig. S6 tempts us to conclude that even the ground state for $U = 8.5t$ in phase II shows strong tendency towards the 120° Néel order. However, we emphasize that the peak structure in $S(\mathbf{q})$ for $U = 8.5t$ in phase II are much smaller and broader than that for $U = 11t$ in phase III. Indeed, as shown in Figs. 3 and 4, the response to the pinning magnetic field and the real-space spin correlation function are clearly different in phases II and III.

6. Hopping amplitude

We also calculate the hopping amplitude $B_{\langle i,j \rangle}$ between nearest-neighbor sites i and j , defined as

$$B_{\langle i,j \rangle} = \frac{1}{2} \langle \psi_0 | (c_{i,\sigma}^\dagger c_{j,\sigma} + c_{j,\sigma}^\dagger c_{i,\sigma}) | \psi_0 \rangle. \quad (\text{s10})$$

The representative results for the three different phases are shown in Fig. S7. We first notice in Figs. S7(a)–S7(c) that the results are invariant under the translation along the y -direction, the reflection about mirror planes perpendicular to the y -direction, and the 180° rotation around the center of the cluster, thus implying that the convergence of our results is satisfactory. For better quantitative comparison, Fig. S7(d) shows $B(l) = B_{\langle i,j \rangle}$ along x -direction for the l -th bond connecting sites i and j (for the indexing of bonds, see Fig. 1 in the main text).

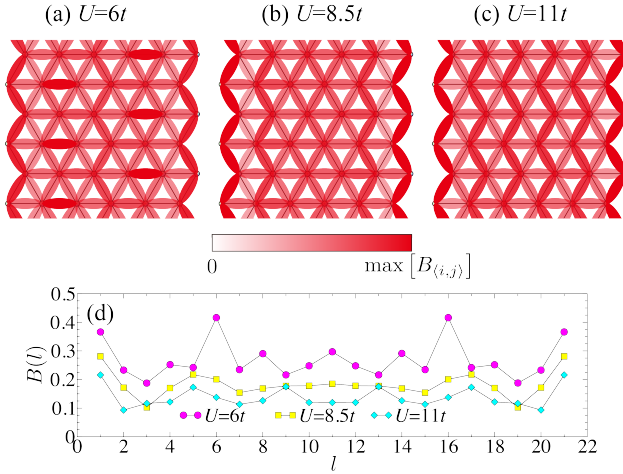


Figure S7. (color online) Intensity plot of nearest-neighbor hopping amplitude $B_{\langle i,j \rangle}$ for (a) $U = 6t$, (b) $U = 8.5t$, and (c) $U = 11t$. Here, $\max[B_{\langle i,j \rangle}]$ is the maximum value of $B_{\langle i,j \rangle}$ for each U . (d) $B(l) = B_{\langle i,j \rangle}$ along x -direction, where the bond index l connecting sites i and j is denoted in Fig. 1. The cluster used here is XC6 shown in Fig. S1(a). Notice that the decrease of kinetic energy, proportional to $-\sum_l B(l)$, is nicely observed with increasing U/t .

We find that $B_{\langle i,j \rangle}$ exhibits the similar oscillation patterns to those observed in $S_{\langle i,j \rangle}$ (see Fig. 5 in the main text). The similarity between $B_{\langle i,j \rangle}$ and $S_{\langle i,j \rangle}$ is expected for large U/t since the kinetic energy, proportional to $B_{\langle i,j \rangle}$, can be in a strong coupling regime transferred to the Heisenberg exchange interaction, which is related to $S_{\langle i,j \rangle}$. However, it is surprising that this similarity is present also in the coupling regimes shown in Fig. S7, where there is in general no direct connection between $B_{\langle i,j \rangle}$ and $S_{\langle i,j \rangle}$. As shown in Fig. S7(d), we find that the oscillations of $B(l)$ around the center of the cluster are most strongly reduced for $U = 8.5t$ (phase II) in comparison to those in phases I and III. This implies that the ground state in phase II is not compatible with the nearest-neighbor valence bond solid.

7. Chiral correlation function

Finally, we calculate the chiral correlation function $\Delta(\Delta_i, \Delta_j)$ defined as

$$\Delta(\Delta_i, \Delta_j) = \langle \psi_0 | C_{\Delta_i} C_{\Delta_j} | \psi_0 \rangle \quad (\text{s11})$$

with

$$C_{\Delta_i} = \vec{S}_{i_1} \cdot (\vec{S}_{i_2} \times \vec{S}_{i_3}), \quad (\text{s12})$$

where Δ_i indicates the i -th elementary triangle formed by three neighboring sites i_1 , i_2 , and i_3 . \vec{S}_i is the spin operator at site i defined as

$$\vec{S}_i = \frac{1}{2} \sum_{\sigma_1=\uparrow,\downarrow} \sum_{\sigma_2=\uparrow,\downarrow} c_{i,\sigma_1}^\dagger \vec{\sigma}_{\sigma_1,\sigma_2} c_{i,\sigma_2}, \quad (\text{s13})$$

where $\vec{\sigma} = (\sigma_x, \sigma_y, \sigma_z)$ are Pauli matrices. Fig. S8 shows the chiral correlation function $\Delta(\Delta_i, \Delta_i + l) = \Delta(l)$ with $\Delta_i = 0$ along x -direction, where the indexing of elementary triangles is indicated in Fig. S1(a). We find that the sign of $\Delta(l)$ exhibits nontrivial oscillation [Fig S8(a)] and the amplitude of $\Delta(l)$ decays exponentially [Fig S8(b)]. Therefore, we can conclude that the chiral spin liquid is most unlikely to be the ground state in phase II [5].

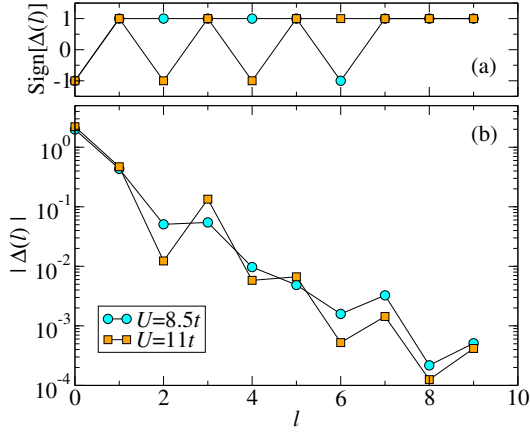


Figure S8. (color online) (a) Sign and (b) amplitude of chiral correlation function $\Delta(l)$ for $U = 8.5t$ and $U = 11t$. The cluster used here is XC6 shown in Fig. S1(a)

- [3] O. I. Motrunich, *Phys. Rev. B* **72**, 045105 (2005).
- [4] M. S. Block, D. N. Sheng, O. I. Motrunich, and M. P. A. Fisher, *Phys. Rev. Lett.* **106**, 157202 (2011).
- [5] S.-S. Gong, W. Zhu, and D. N. Sheng, *Sci. Rep.* **4**, 6317 (2014).